A Dynamical Approach to the Spatio-temporal Features of the Portevin-Le Chatelier Effect

G.Ananthakrishna[1]

Abstract: We show that the extended Ananthakrishna's model exhibits all the features of the Portevin - Le Chatelier effect including the three types of bands. The model reproduces the recently observed crossover from a low dimensional chaotic state at low and medium strain rates to a high dimensional power law state of stress drops at high strain rates. The dynamics of crossover is elucidated through a study of the Lyapunov spectrum.

keyword: PLC effect,Chaos,Power laws,PLC bands

1 Introduction

Of the dislocation patterns seen under different modes of deformation, the most complex is the Portevin - Le Chatelier (PLC) effect. The PLC effect is observed when certain metallic alloys are deformed in a tension test in a range of strain rates and temperatures. Here a uniform deformation mode becomes unstable leading to spatially and temporally inhomogeneous state. Each stress drops is associated with the nucleation and often the propagation of a band of localized plastic deformation. In polycrystals, on increasing strain rates or decreasing the temperature, one first finds the type C, identified with randomly nucleated static bands with large characteristic stress drops. Then the correlated 'hopping' type B bands are seen with serration amplitudes smaller than the type C. Finally, one observes continuously propagating type A bands associated with small stress drops. (In single crystals such a clear classification does not exist.) These different types of PLC bands are believed to represent distinct correlated states of dislocations in the bands.

The classical explanation of the PLC effect is through dynamic strain aging (DSA) first suggested by Cottrell (1) and later improved by others (see Ref. (2)). DSA refers to the interaction of mobile dislocations with diffusing solute atoms. At low strain rates (or high temperatures) the average velocity of dislocations is low, there is sufficient time for solute atoms to diffuse to the dislocations and pin them. Longer they are arrested, larger will be the stress required to unpin them. When dislocations are unpinned, they move at large speeds till they are pinned again. At high strain rates (or low temperatures), there is insufficient time for the solute atoms to diffuse to the dislocations and hence the stress required to unpin them decreases. Thus, in a range of strain rates and temperatures where these two time scales are of the same order, the PLC instability manifests. The competition between the slow rate of pinning and sudden unpinning of the dislocations, at the macroscopic level, translates into a negative strain rate sensitivity (SRS) of the flow stress as a function of strain rate which is the basic instability mechanism used in most phenomenological models (2).

The inherent nonlinearity and the presence of multiple time scales necessitates the use of tools and concepts of nonlinear dynamical systems for a proper understanding of this phenomenon. The first dynamical approach was taken in mid 80s by Ananthakrishna and coworkers(3). The model uses three types of dislocation densities taken to represent collective degrees of freedom of dislocations. Apart from predicting the generic features of the PLC effect, such as the emergence of the negative SRS (3; 4), the existence of critical strain for the onset of the PLC instability, and the existence of a window of strain rates and temperatures for the occurrence of the PLC effect (see (3)), one prediction that is specific to the model is the existence of chaotic stress drops is a range of strain rates (5) subsequently verified using methods of time series analysis (5; 6; 7). More recent studies report an intriguing crossover from a low dimensional chaotic state found at medium strain rates to a power law state of stress drops observed at high strain rates (8; 9). A chaotic state involves small number of degrees of freedom, characterized by self-similarity of the attractor and sensitivity to initial conditions. In contrast, the power-law state of distributions of amplitudes and durations of avalanches is an

[1] Materials Research Centre and Centre for Condensed Matter Theory, Indian Institute of Science, Bangalore-560012, India

infinite dimensional state. Though the power law state is reminiscent of self-organized criticality (SOC) (10) is however seen at low drives unlike the present case. Indeed, the PLC effect is one the two rare phenomenon where such a crossover is seen, the other being in hydrodynamic turbulence (11), thus making the study of the PLC effect all the more interesting and important. In this paper, we present an extension of the Ananthakrishna's model to explain this crossover in the PLC effect as well as different types of bands.

2 The Ananthakrishna's Model

The fully dynamical basis of the dynamical model makes it most suitable for studying this crossover. Here, we outline the model in terms of scaled variables in the notation of Ref. (4) and introduce a spatial coupling arising out of the cross-slip mechanism (2). The model consists of densities of mobile, immobile, and Cottrell's type dislocations denoted by $\rho_m(x,t)$, $\rho_{im}(x,t)$ and $\rho_c(x,t)$ respectively, in the scaled form. The evolution equations are:coupled to stress rate equation through

$$\begin{aligned}\frac{\partial \rho_m}{\partial t} &= -b_0\rho_m^2 - \rho_m\rho_{im} + \rho_{im} - a\rho_m + \phi_{eff}^m\rho_m \\ &+ \frac{D}{\rho_{im}}\frac{\partial^2(\phi_{eff}^m(x)\rho_m)}{\partial x^2}, \quad (1)\end{aligned}$$

$$\frac{\partial \rho_{im}}{\partial t} = b_0(b_0\rho_m^2 - \rho_m\rho_{im} - \rho_{im} + a\rho_c), \quad (2)$$

$$\frac{\partial \rho_c}{\partial t} = c(\rho_m - \rho_c), \quad (3)$$

$$\frac{d\phi(t)}{dt} = d[\dot{\varepsilon} - \frac{1}{l}\int_0^l \rho_m(x,t)\phi_{eff}^m(x,t)dx] = d[\dot{\varepsilon} - \dot{\varepsilon}_p] \quad (4)$$

The first term in eqn.(1) refers to annihilation or immobilization of two mobile dislocations, the second term to the annihilation of a mobile dislocation with an immobile one, and the third term to the remobilization of the immobile dislocation due to stress or thermal activation. The fourth term represents the immobilization of mobile dislocations due to solute atoms. Once a mobile dislocation starts acquiring solute atoms we regard it as the Cottrell's type dislocation ρ_c. As they progressively acquire more solute atoms, they eventually stop, then they are considered as immobile dislocations ρ_{im}. Alternately, the aggregation of solute atoms can be regarded as the definition of ρ_c, ie., $\rho_c = \int_{-\infty}^{t} dt' \rho_m(t')K(t-t')$. For the sake of simplicity, we use a single time scale with $K(t) = e^{-ct}$ (see ref. (4)). The fifth term represents the rate of multiplication of dislocations due to cross-slip. This depends on the velocity of the mobile dislocations taken to be $V_m(\phi) = \phi_{eff}^m$, where $\phi_{eff} = (\phi - h\rho_{im}^{1/2})$ is the scaled effective stress, ϕ the scaled stress, m the velocity exponent and h a work hardening parameter. Cross-slip is a natural source of spatial coupling within the scope of the model, as dislocations generated due to cross slip at a point spread over to the neighboring elements. (See Ref. (2) for other sources of coupling.) Let Δx be an elementary length. Defining $\Phi(x) = \rho_m(x,t)\phi_{eff}^m(x,t)$, and considering dislocation multiplication occurring $x \pm \Delta x$ and x, the rate of mobile density is given by $\Phi(x) + \frac{p}{2}[\Phi(x+\Delta x) - 2\Phi(x) + \Phi(x-\Delta x)]$. Here p is the probability of cross-slip spreading into neighboring elements. Expanding $\Phi(x \pm \Delta x)$ and keeping the leading terms, we get $\dot{\rho}_m(x,t) = \rho_m V_m + \frac{p}{2}\frac{\partial^2(\rho_m V_m)}{\partial x^2}(\Delta x)^2$. Noting that cross-slip spreads only into regions of minimum back stress and that the back stress is usually taken to result from the immobile dislocation density ahead of it, we use $\Delta x^2 = <\Delta x^2> = \bar{r}^2\rho_{im}^{-1}$. Here $<\ldots>$ refers to the ensemble average and $\bar{r}^2$ is an elementary (dimensionless) length. In Eq.(4), $\dot{\varepsilon}$ is scaled applied strain rate and $\dot{\varepsilon}_p$ the plastic strain rate. Finally, a, b_0, c and d are respectively the scaled rate constants referring, respectively, to the concentration of solute atoms slowing down the mobile dislocations, the thermal and athermal reactivation of immobile dislocations, and the rate at which solute atoms are gathering around the mobile dislocations and the combined elastic constant of machine and the sample.

The PLC state is reached through a Hopf bifurcation. The domain of instability in $\dot{\varepsilon}$ is $10 < \dot{\varepsilon} < 2000$ when the values of other parameters are in the instability limit. Here, we use $a = 0.8, b_0 = 0.0005, c = 0.08, d = 0.00006, m = 3.0, h = 0.07$ and $D = 0.5$. But the results hold true for a wide range of other parameters in the instability domain including a range of values of D. A uniform steady state exists beyond this domain.

The above equations are discretized by considering the specimen to be divided into N equal parts of some unit length. Then, $\rho_m(j,t)$, $\rho_{im}(j,t), \rho_c(j,t)$, $j = 1,...N$, and $\phi(t)$ are solved. Due to the widely differing time scales, appropriate care is exercised in the numerical solutions by using a variable step fourth order Runge-Kutta scheme. The spatial derivative is approximated by its central difference. The initial values are taken as the steady state values for the variables (as the long term evo-

lution does not depend on the initial values) with a Gaussian spread along the length of the sample. Now consider the boundary conditions. Since the sample is strained at the grips, we use high (two orders of magnitude more than the rest of the sample) values of $\rho_{im}(j,t)$, $j = 1$ and N. Further, as bands cannot propagate into the grips, we use $\rho_m(j,t) = \rho_c(j,t) = 0$ at $j = 1$ and N.

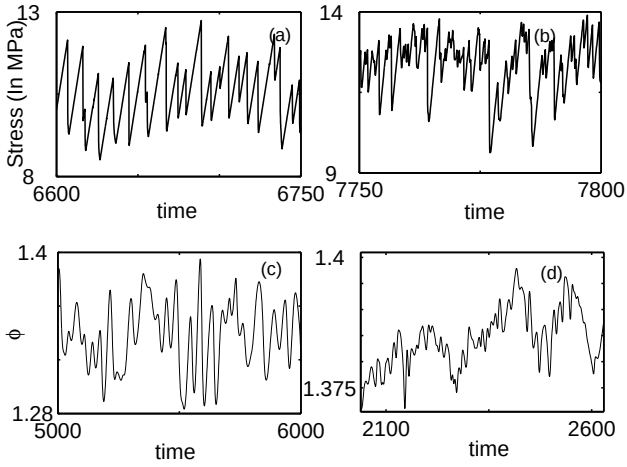

Figure 1 : (a,b) Experimental stress-time series for the chaotic state at $\dot{\varepsilon}_a = 1.7 \times 10^{-5} s^{-1}$ and power law state at $\dot{\varepsilon}_a = 8.3 \times 10^{-5} s^{-1}$. (c, d) Stress-time series from the model at $\dot{\varepsilon} = 120$ and $\dot{\varepsilon} = 280$ respectively.

3 Dynamics of Crossover

3.1 Reconstruction of Dynamics from Experimental Time Series

Plots of two experimental stress-strain curves corresponding to the chaotic (medium $\dot{\varepsilon}$) and power law regimes of applied strain rates (high $\dot{\varepsilon}$) and time series from the model at intermediate and high strain rates are shown in Fig. 1. The similarity of the experimental time series at medium and high strain rates with that of the model in similar range of $\dot{\varepsilon}$ is clear. Now consider the dynamical aspects of the experimental time series. It was shown earlier (8) that the stress-strain curve in Fig. 1 a is chaotic. This was done by demonstrating the existence of a finite correlation dimension (12) and the existence of a positive Lyapunov exponent (13). The correlation dimension, ν, of the experimental attractor for this value of $\dot{\varepsilon}_a$ was found to be 2.3. Then, the number of degrees of freedom required for the description of the dynamics of the system is given by the minimum integer larger than $\nu + 1$ which is four in this case, consistent with that used in the original model. The geometrical interpretation of these degrees of freedom is that it is the subspace to which the trajectories are confined. The dimension of this subspace can be obtained directly by a method called as the singular value decomposition (14). This method has an *additional advantage* of allowing the *visualization of the strange attractor*. (See (7) where this method has been applied to the PLC time series.) In this method, the trajectory matrix is constructed and the eigen values of the covariance matrix are calculated. For this case, the relative strength of the fourth eigen value drops more than two orders of magnitude compared to the first and changes very little beyond the fourth (15). Thus, the dimension of the experimental attractor is four consistent with that obtained from the correlation dimension. Using the first three principal directions of the subspace $C_i; i = 1$ to 3, we have reconstructed the experimental attractor in the space of specifically chosen directions $C_1 - C_2, C_3$ and C_1 to permit comparison with the model. This is shown in Fig. 2a. The strange attractor obtained from the model in the space of ρ_m, ρ_{im} and ρ_c (at an arbitrary spatial location, here $j = 50$ and $N = 100$) is shown in Fig. 2b for $\dot{\varepsilon} = 120$ corresponding to the mid chaotic region. Clearly, *the geometry of the two attractors are similar particularly along the direction of the arrow* (Fig. 2a) identified with the loading direction in Fig. 1a.

3.2 Power Law State of Stress Drops

Consider the stress-time series at high strain rates beyond $\dot{\varepsilon} \sim 260$, say 280, shown in Fig. 1 obtained from the model. It is clear that there are stress drops of all magnitudes. Actually, the distribution of stress drop magnitudes, $D(\Delta\phi)$, shows a power law $D(\Delta\phi) \sim \Delta\phi^{-\alpha}$. This is shown in Fig. 3 ($\circ$) along with the experimental points ($\bullet$) corresponding to $\dot{\varepsilon}_a = 8.3 \times 10^{-5} s^{-1}$. It is clear from Fig. 3 that both experimental and theoretical points show a scaling behavior with an exponent value $\alpha \approx 1.1$ (Fig. 1a). The distribution of the durations of the stress drops $D(\Delta t) \sim \Delta t^{-\beta}$ also follows a power law with an exponent value $\beta \approx 1.3$.

3.3 Dynamical Characterization of the Model

A natural tool for characterizing the crossover is to study the distribution of Lyapunov exponents λ_i $(i = 1, .., M = 3N + 1)$ using Eqs. (1-4) for the entire range of strain

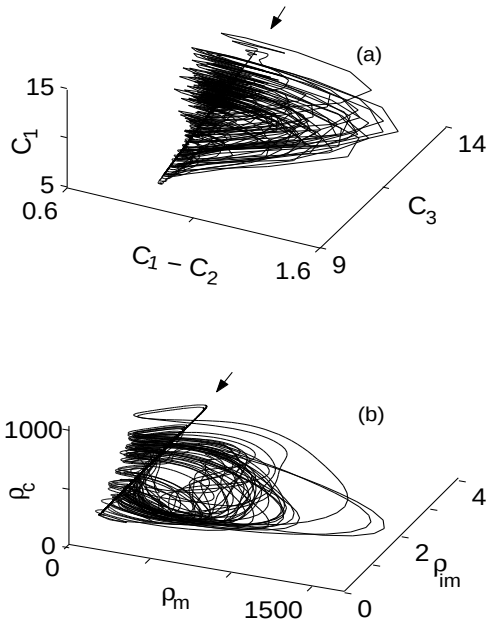

Figure 2 : (a) Reconstructed experimental attractor (b) Attractor from the model for $N = 100$, $j = 50$.

rates. The largest Lyapunov exponent (LLE) is shown in Fig. 4a as a function of the strain rate for $N = 100$. The region of chaos is seen to be $35 < \dot{\varepsilon} < 250$ beyond which the LLE almost vanishes ($\sim 5 \times 10^{-4}$). This region of strain rates beyond 250, as we will show corresponds to the power law regime of stress drops. Now, consider the evolution of the distribution of Lyapunov exponents as a function of $\dot{\varepsilon}$ as we move from the chaotic and the power law regime. In the chaotic region, the distribution of Lyapunov exponents is quite broad. A plot for $\dot{\varepsilon} = 120$ is shown Fig. 4b. As $\dot{\varepsilon}$ increases to 280, concomitant with the decrease in the maximum Lyapunov exponent to a small value, $\approx 5.2 \times 10^{-4}$, the number of null exponents (almost vanishing) *increases gradually* reaching a value $\approx 0.38M$ in the range $[-0.00052, 0.00052]$ (compared to only a few for $\dot{\varepsilon} = 120$). For $\dot{\varepsilon} \geq 250$, below a resolution $\sim 10^{-4}$, most cross each other as a function of time, but the (time averaged) distribution remains unaffected. The finite density of null exponents has a peaked nature in the interval $250 \leq \dot{\varepsilon} \leq 700$. A plot is shown in Fig. 4c for $\dot{\varepsilon} = 280$ which can be fitted to a power law $D(|\lambda|) \sim |\lambda|^{-\gamma}$ as shown in Fig. 4d with $\gamma = 0.6$. Thus, the spectrum changes from *a set of both positive and negative, but few null exponents* in the chaotic region, to *a dense set of null exponents and negative exponents with no positive exponents* in the scaling regime. As null exponents correspond to a marginal situation, their finite density in the power law state implies that most spatial elements are perpetually close to the marginal state of unpinning. Indeed, a full analysis confirms the the correctness of the edge of unpinning picture (16).

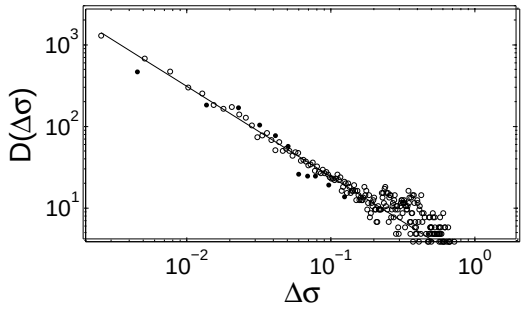

Figure 3 : Distributions of the stress drops from the model (∘), from experiments (•) for $N = 1000$ and $\dot{\varepsilon} = 280$. Solid line is a guide to the eye.

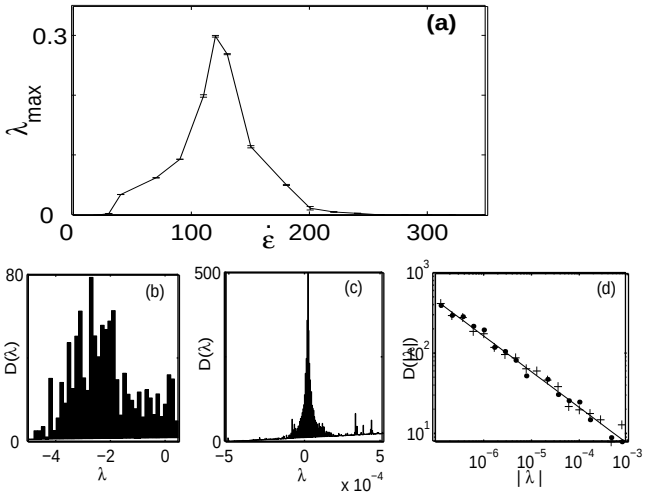

Figure 4 : (a)The largest Lyapunov exponent of the model.(b) Distribution of the Lyapunov exponents at $\dot{\varepsilon} = 120$ for $M = 1051$. (c) and (d) Distribution of the null exponents at $\dot{\varepsilon} = 280$ for $M = 10000$. In (d) (+) refers to positive and (•) to negative null Lyapunov exponents.

4 Formation and Propagation of Bands

We now consider the nature the PLC bands seen in our model. Most models of bands use diffusive coupling although the physical mechanism of the term is different

(2). An important difference in our model is the presence of the factor $1/\rho_{im}$ in the spatial coupling that accounts for spreading of dislocations into regions of low back stress. Further, this type of spatial term couples length scales and time scales in a dynamical way as ρ_{im} itself evolves in time, leading to changes in the time scale of internal relaxation as a function of $\dot{\varepsilon}$. We expect this to lead to changes in spatial correlation as strain rate is increased.

In the region where chaotic and power law states are observed, the nature of bands can be broadly classified into three different types occurring at low, intermediate and high strain rates.

For strain rates, $30 \leq \dot{\varepsilon} < 70$, we get uncorrelated static dislocation bands shown in Fig. 5 (top) for a typical value, say for $\dot{\varepsilon} = 40$. The associated stress-time curves which are nearly regular have large characteristic stress drops. At slightly higher values of strain rates, $70 \leq \dot{\varepsilon} < 180$, we find that new bands nucleate ahead of the earlier ones, giving a visual impression of *hopping bands* (Fig. 5 middle). A plot of $\rho_m(j,t)$ shown for $\dot{\varepsilon} = 130$ displays the hopping nature. However, this hopping motion does not continue till the other boundary. They stop midway and another set of hopping bands reappear in the neighborhood. Stress-time plots in this regime have a form similar to Fig. 1a. As the strain rate is increased further, the extent of propagation increases, concomitantly, the magnitudes of the stress drops decrease. We see continuously propagating bands even at $\dot{\varepsilon} = 240$ from one end to the other as can be seen from Fig. 5 (bottom). The stress -strain curves in this region of strain rates, exhibit scale free feature in the amplitude of the stress drops (Fig. 1 d) with a large number of small drops. The large stress drops correspond to bands having reached the end of the specimen.

It is possible to calculate the velocity of the propagating bands in the high strain rate limit. The coupled set of integro-partial differential equations can be to reduced to the standard form of Fischer-Kolmogorov equation for propagative fronts. Using marginal stability analysis, we get the velocity of the bands

$$v = 2\sqrt{\frac{D\dot{\varepsilon}}{\overline{\rho}_m \rho_{im}}\left(\frac{\dot{\varepsilon}}{\overline{\rho}_m} - a - \rho_{im}\right)}. \qquad (5)$$

At high applied strain rate, we note that $\overline{\rho}_m \sim \overline{\rho}_m^*$, the fixed point value which can be assumed to be constant.

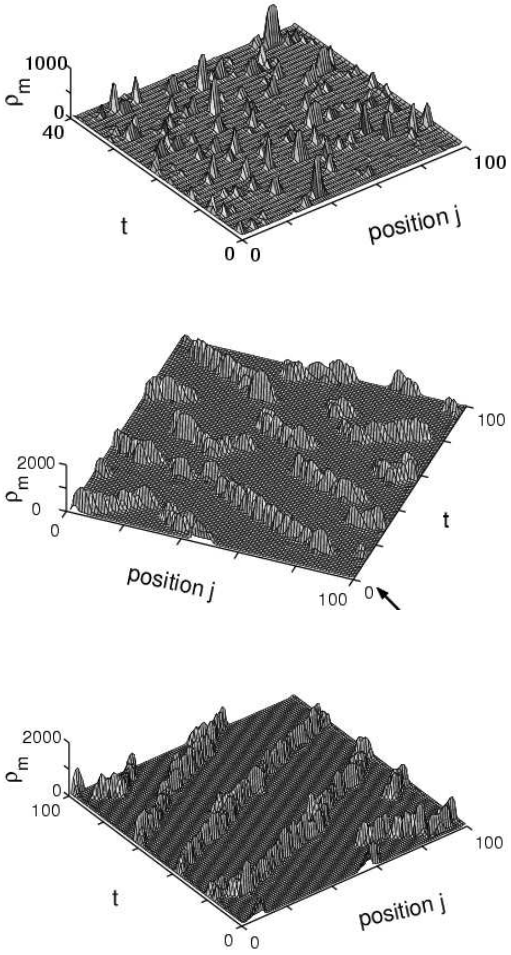

Figure 5 : From top to bottom: spatially uncorrelated bands at $\dot{\varepsilon} = 40$, the hopping bands at $\dot{\varepsilon} = 130$ and the propagative band at $\dot{\varepsilon} = 240$.

Thus, the velocity of the bands is proportional to the applied strain rate, a result similar to Ref. (17) which has been verified numerically as well. In the unscaled units, the band velocity $\sim 120\mu m/s$ corresponding to scaled strain rate $\dot{\varepsilon} = 260$, again consistent with the experimental values (17). Further, $v \propto \overline{\rho}_m^{-1}$ which also appears to be consistent with an old experimental result.

We note here that the hopping type bands belong to the chaotic regime, a result consistent with the recent studies on Cu-Al polycrystals (9). On the other hand, the propagating bands are seen in the power law regime of stress drops (18), again consistent with these studies (8; 9). Curiously the uncorrelated bands predicted by the model also belong to the chaotic regime.

5 Discussion and Conclusions

Several comments may be in order on the dynamics of the crossover. The crossover itself is smooth as the changes in the Lyapunov spectrum are gradual. Second, the power law here is of purely dynamical origin.Third, our analysis shows that the power law regime of stress drops occurring at high strain rates belongs to a different universality class compared to the well know self-organized criticality (10) seen at low drives, as our system is characterized by a dense set of null exponents. As zero exponents correspond to a marginal situation, their finite density physically implies that most spatial elements are close to criticality. Indeed, we have visualized the configurations of dislocation in the scaling regime of stress drops (ie., $\dot{\varepsilon} > 260$) using *the slow manifold* analysis (16; 15) which shows that most dislocations are at the threshold of unpinning. More significantly, the dense set of null Lyapunov exponents themselves follow a power law. Further, we note that the Lyapunov spectrum evolves from a set of both positive and negative, but few null exponents in the chaotic region, to a dense set of marginal exponents as we reach the power law regime. Thus, the dense set of null exponents in our model is actually similar to that obtained in shell models of turbulence where the power law is seen at high drive values (19).

In summary, the original model extended to include the spatial degrees of freedom explains the crossover in the dynamics from chaotic to power law regime as observed in experiments. The model also exhibits all the three types of bands, namely, the uncorrelated, hopping and the continuously propagating type bands as strain rate is increased as in experiments (16). Thus, the extended Ananthakrishna's model captures the complex spatio-temporal dynamics of the PLC effect. Finally, as far as we know, this is first fully dynamical model which exhibits a crossover from chaotic to power law regime in the general context of dynamical systems and should be of interest to the area of dynamical systems.

The author wishes to thank Dr. M. S. Bharathi for the collaborative work. This work is supported by Department of Science and Technology, New Delhi, India.

References

[1]A. H. Cottrell, *Dislocations and Plastic Flow in Crystals* (Clarendon Press, Oxford, 1953).

[2]L.P. Kubin, C. Fressengeas and G. Ananthakrishna, in *Collective Behavior of Dislocations*, edited by F.R.N. Nabarro and M.S. Deusbery, *Dislocations in Solids* Vol.11 (North-Holland, Amsterdam, 2002).

[3]G. Ananthakrishna and M.C. Valsakumar, J. Phys. D. **15**, L171 (1982).

[4]S. Rajesh and G. Ananthakrishna, Phys. Rev. E. **61**, 3664 (2000); Physica D **140**, 193 (2000).

[5]G. Ananthakrishna and M.C. Valsakumar, Phys. Lett. **A95**, 69 (1983).

[6]G. Ananthakrishna *et al.*, Scripta. Metall. **32**, 1731 (1995).

[7]S.J. Noronha, *et al.*, Int. Jl. of Bifurcation and Chaos **7**, 2577 (1997).

[8]G. Ananthakrishna *et al.*, Phys. Rev. E. **60**, 5455 (1999).

[9]M.S. Bharathi, *et al.*, Phys. Rev. Lett. **87**,165508 (2001).

[10]P. Bak, C. Tang and K. Wiesenfeld, Phys. Rev. Lett. **59**, 381 (1987); Phys. Rev. A. **38**, 364 (1988).

[11]See for instance F. Heslot, B. Castaing and A. Libchaber, Phys. Rev. A. **36**, 5780 (1987).

[12]P. Grassberger and I. Procaccia, Physica D **9**, 189 (1983).

[13]H.D.I. Abarbanel, *Analysis of Observed Chaotic Data* (Springer-Verlag, New York, 1996).

[14]D. Broomhead and G. King, Physica. **20D**, 217 (1987).

[15]G. Ananthakrishna and M. S. Bharathi, To appear in Phys. Rev. E (2004).

[16]M.S. Bharathi, S. Rajesh and G. Ananthakrishna, Scripta Materialia, **48**, 1355 (2003).

[17]P. Hähner et al., Phys. Rev. B **65**,134109 (2002);

[18]M. S, Bharathi and G. Ananthakrishna, Phys. Rev. E **67**, 065104R (2003).

[19]M. Yamada and K. Ohkitani, J. Phys. Soc. Jpn. **56**, 4210 (1987); A. Cristani *et al*, Physica D, **76**, 239 (1994) and the references therein.